



HAL
open science

Processing of CaLa₂S₄ infrared transparent ceramics: A comparative study of HP and FAST/SPS techniques

Guillaume Durand, Quentin Bizot, Nathalie Herbert, Samuel Quéméré,
Mathieu Pasturel, Xiang-Hua Zhang, Odile Merdrignac-Conanec

► To cite this version:

Guillaume Durand, Quentin Bizot, Nathalie Herbert, Samuel Quéméré, Mathieu Pasturel, et al.. Processing of CaLa₂S₄ infrared transparent ceramics: A comparative study of HP and FAST/SPS techniques. *Journal of the American Ceramic Society*, 2020, 103 (4), pp.2328-2339. 10.1111/jace.16918 . hal-02436627

HAL Id: hal-02436627

<https://univ-rennes.hal.science/hal-02436627v1>

Submitted on 7 Apr 2023

HAL is a multi-disciplinary open access archive for the deposit and dissemination of scientific research documents, whether they are published or not. The documents may come from teaching and research institutions in France or abroad, or from public or private research centers.

L'archive ouverte pluridisciplinaire **HAL**, est destinée au dépôt et à la diffusion de documents scientifiques de niveau recherche, publiés ou non, émanant des établissements d'enseignement et de recherche français ou étrangers, des laboratoires publics ou privés.

Processing of CaLa_2S_4 infrared transparent ceramics: a comparative study of HP and FAST/SPS techniques

Guillaume R. Durand, Quentin Bizot, Nathalie Herbert, Samuel Quéméré, Mathieu Pasturel, Xiang-Hua Zhang, Odile Merdrignac-Conanec

Univ Rennes, CNRS, ISCR (Institut des Sciences Chimiques de Rennes) - UMR 6226, F-35000 Rennes, France

Correspondence

Odile Merdrignac-Conanec, Institut des Sciences Chimiques de Rennes, UMR CNRS 6226, Equipe Verres et Céramiques, Université de Rennes1, Campus de Beaulieu, 35042 Rennes Cedex, France
Email : odile.merdrignac@univ-rennes1.fr

Abstract

The densification of CaLa_2S_4 (CLS) powders prepared by combustion method was investigated by the use of Field Assisted Sintering Technique (FAST) and Hot Pressing (HP). CLS powders were sintered using FAST at 1000°C at different pressures and heating rates and sintered by HP under 120 MPa from 800°C to 1100°C for 6 h with a heating rate of $10^\circ\text{C}\cdot\text{min}^{-1}$. Comparison of both techniques was further realized by use of the same conditions of pressure, dwell time and heating rate. Complementary techniques (XRD, SEM-EDS, density measurements, FT-IR spectroscopy) were employed to correlate the sintering processes/parameters to the microstructural/compositional developments and optical transmission of the ceramics. Both sintering techniques produce ceramics with sub-micron grain size and relative density of about 99 %. Nevertheless, HP is more suitable to densify CLS ceramics without fragmentation and also reach higher transmission than FAST. Transmission of 40-45% was measured out of a possible maximum of 69% based on the Fresnel losses in the 8-14 μm window when HP is applied at 1000°C for 6 h under 120 MPa. In both techniques, ceramics undergo reduction issues that originate from graphitic sintering atmosphere.

1. INTRODUCTION

In the early 1980s, compounds of the CaLa_2S_4 - La_2S_3 solid solution system (CLS) with broad transmission domain from 0.5 to 14 μm , cubic structure, high melting point (1810°C) and high hardness, emerged as alternative materials to the reference infrared (IR) multispectral material ZnS for infrared windows and domes. ZnS has significant absorption beyond 11 μm and sintering temperature limitation to retain the isotropic cubic structure (sphalerite/wurtzite phase transition occurs at 1020°C).

Furthermore, ZnS ceramics are currently available at a very high cost as they are produced using the long and complex Chemical Vapor Deposition (CVD, IR grade) and Hot Isostatic Pressing (HIP, Multispectral grade) techniques¹. ZnS has also a poor resistance to erosion (by water, sand or dust) due to low hardness (HK (ZnS-CVD) = 210-240 kg.mm⁻² / HK (ZnS-Multispectral) = 150-160 kg.mm⁻²)² and fracture toughness. With a hardness double that of ZnS, (HK (CLS) = 570 kg.mm⁻²)², CLS has a better erosion resistance to withstand harsh environments. Moreover, a higher transparency in the far infrared region (up to 14 μm) significantly enhances the performance of the infrared optical systems and allows the use of uncooled detectors resulting in a significant reduction in system cost¹⁻⁴. The fabrication of polycrystalline CLS ceramics has been originally explored through ceramic routes by the Naval Weapons Center in conjunction with Raytheon (USA) and the Royal Signals and Radar Establishment (UK)⁵. Optics of good quality were obtained but reproducibility issues impeded subsequent development.

Most of the CLS powders synthesis methods found in literature consist in a two-step process. The first step is the synthesis of CLS precursors containing intimately mixed calcium and lanthanum ions, which could be either mixed oxides^{4, 6}, co-precipitated carbonates^{2, 7-10}, spray-pyrolysed mixed oxides (Evaporative Decomposition of Solutions (EDS) method)^{3, 11-17} or alcoxides¹⁸⁻²². These precursors are subsequently sulfurized in H₂S¹²⁻¹⁵ or CS₂²²⁻²⁴ atmosphere and converted into pure CLS powders. Sintering of the powders is thereafter carried out by different sintering techniques: Hot Pressing (HP)^{4, 6, 24-26}, natural sintering in sulfurizing atmosphere followed by Hot Isostatic Pressing (HIP)^{2, 3, 12, 27} or Field Assisted Sintering Technique (FAST also denominated as Spark Plasma Sintering) for which, to the best of our knowledge, only two references have been published very recently^{28, 29}.

Reduction phenomena of CLS at high sintering temperatures, namely T ≥ 1000°C, are generally reported issues for sintered CLS ceramics^{4, 6, 10, 13}. CLS are compounds of the ternary cubic system formed by CaLa₂S₄, γ-La₂S₃ and La₃S₄^{3, 30-35}. These phases are isostructural (cubic Th₃P₄, space-group $I\bar{4}3d$) and derive from γ-La₂S₃ which has a lacunar cationic lattice (La_{8/3}[□]_{1/3}S₄). The filling of cationic vacancies of γ-La₂S₃ with Ca²⁺ or La³⁺ ions leads to the formation of isostructural compounds, respectively CaLa₂S₄ and La₃S₄. All compounds of the CaLa₂S₄-γ-La₂S₃ binary join are transparent while those of CaLa₂S₄-La₃S₄³⁶ are black and metallic^{33-35, 37} (they are noted La₃S₄:Ca for simplification). Note these structural specificities of the ternary system are a major cause for the

sensitivity of CLS materials to reduction and blackening at high temperature. To limit the tendency of CLS to drift off stoichiometry in graphitic atmosphere, the sintering must proceed at low temperature.

The present work investigates the densification by means of FAST/SPS and HP techniques of CLS powders prepared according to our previously reported combustion synthesis method^{25, 38}. The main objective of this study is to evaluate FAST/SPS technique ability to densify the aforementioned CLS powders, in comparison to conventional HP. Note that sintering by FAST is assessed for the first time on combusted CLS powders. The microstructure/composition and subsequent optical properties of the ceramics are fully evaluated and compared.

2. EXPERIMENTAL PROCEDURES

2.1. Powders synthesis and ceramics processing

CLS powders were prepared using a solution combustion method followed by a sulfurization step³⁸. Calcium nitrate $\text{Ca}(\text{NO}_3)_2 \cdot 4\text{H}_2\text{O}$ (Alfa Aesar, 99.99 %), lanthanum nitrate $\text{La}(\text{NO}_3)_3 \cdot 6\text{H}_2\text{O}$ (Alfa Aesar, 99.99 %) and thioacetamide (TAA) CH_3CSNH_2 (Sigma Aldrich, ≥ 99 %, ACS Reagent) were used as starting materials. According to previous work³⁶, initial La/Ca ratio was 2.3 to ensure the formation of a pure CLS phase. As-combusted powders were crushed in agate mortar and subsequently heat-treated in pure H_2S flow in a tubular furnace at 1000°C for 4 h. Sulfurized powders were de-agglomerated by grinding in agate mortar and pestle. No other comminution technique was used to avoid contamination of the powders by the grinding materials⁶. All batches were prepared in the same conditions and XRD and FTIR analysis was conducted to ensure consistency from batch to batch.

FAST sintering was performed under dynamic vacuum (about 0.01 mbar) using a HP-D-10 FCT System GmbH (Germany) equipment. A typical quantity of 3 g of powder was introduced in a 20 mm diameter graphite die lined with a 0.2 mm thick Papyex® graphite foil and mounted into the SPS equipment. A standard procedure of 3 ms pulse sequence for the DC current was chosen for the sintering process. The temperature of the SPS furnace was measured using a thermocouple placed inside the graphite die, close to the sample. Powders were sintered at 1000°C under uniaxial pressures of 12, 40, 60 and 80 MPa (maximum recommended pressure on SPS quality graphite) applied from the beginning of the sintering cycle to the end of the dwell time with heating rates of 10, 50, 150, 250 and $350^\circ\text{C} \cdot \text{min}^{-1}$. Dwell time at 1000°C was determined by the end of the displacement of punches and varied from

3.5 min to 27 min. At the end of the sintering process, the pressure was released, then the DC pulses were shut down. Some experiments were performed with a controlled cooling rate of $10^{\circ}\text{C}\cdot\text{min}^{-1}$.

Hot Pressing was carried out under dynamic vacuum (about 0.2 mbar) using VAS (Vide et Appareillages Scientifiques - France) equipment. A typical quantity of 2 g of powder was introduced in a 13 mm diameter graphite die coated beforehand with boron nitride BN (Alfa Aesar 99.5 %) to facilitate demolding. Powders were sintered at 800°C , 900°C , 1000°C and 1100°C with a heating rate of $10^{\circ}\text{C}\cdot\text{min}^{-1}$. A load of 120 MPa (maximum pressure allowed on HP die) was applied at the selected sintering temperature (800 - 1100°C) for 6 h. At the end of the dwell time, the pressure was released and samples were cooled naturally. Graphite grade used in HP experiments was selected to optimize the compressive strength; that used in FAST experiments was selected to optimize electrical conductivity. Also, HP dies were designed for the use of BN coating while FAST dies were designed for the use of graphite foil.

To compare with FAST, some HP sintering experiments were performed in a 20 mm diameter graphite die, under 80 MPa applied from the beginning of the sintering cycle to the end of the dwell time at 1000°C with heating rates of $10^{\circ}\text{C}\cdot\text{min}^{-1}$ and $50^{\circ}\text{C}\cdot\text{min}^{-1}$. FAST and HP ceramic samples, optically polished after a final step with $0.5\ \mu\text{m}$ alumina powder, were respectively 1.4 and 1.9 mm thick. Thickness of HP samples was reduced to 1.4 mm for optical transmission comparison.

2.2. Characterization

X-Ray Diffraction (XRD) patterns were collected at room temperature using a PANalytical X'Pert Pro diffractometer (Cu $K\alpha$ radiation, $\lambda = 1.5425\ \text{\AA}$, 40 kV, 40 mA, PIXcel 1D detector (strip detector: 255pixel $0.013^{\circ}2\theta/\text{px}$)). Routine analysis was performed in the 2θ range 5 - 90° with a step size of 0.026° and a scan time per step of 40 s. Fourier Transform Infra-Red (FTIR) spectroscopy was carried out with a Nicolet 380 FT-IR spectrometer (Thermo Electron Corporation) in the 400 - $4000\ \text{cm}^{-1}$ range. Powder samples were pelleted after careful grinding with anhydrous KBr (99+%, FT-IR grade, Sigma-Aldrich) and compared with freshly prepared blank KBr pellets. Infrared transmission spectra of the ceramics were measured using a Bruker – Vector 22 FT-IR spectrometer in the 2 - $20\ \mu\text{m}$ range on polished samples (optical finishing with $0.5\ \mu\text{m}$ alumina powder in water suspension followed by ultrasonic cleaning in distilled water then in ethanol). Note CLS has a refractive index $n \approx 2.5$ at $10\ \mu\text{m}$ ^{39,40} which gives a theoretical maximum transmission of 69 %.

A FlowSorb II 2300 Micromeritics apparatus was used to determine the Specific Surface Area (SSA) of the powders by the Brunauer-Emmett-Teller single point method. Before measurement, the samples were outgassed in N₂/He flow at 250°C for 30 min. Particle-size distribution analysis using laser-diffraction was performed with a CILAS 1180 particle size analyzer. Powders were dispersed in water, using sodium hexametaphosphate as dispersing agent, and ultrasonicated during analysis.

Powders morphology and ceramics microstructure were examined by Scanning Electron Microscopy (SEM) with a JEOL JSM IT300 equipment (CMEBA, university of Rennes 1). Prior to SEM observations, the samples were metallized with Au-Pd. Powders characterizations were made on the hand-ground powders. The elemental composition of the samples was analyzed by Energy Dispersive Spectroscopy (EDS, Oxford Aztec) attached to the SEM, on polished and ultrasonically cleaned samples, before thermal etching. Grain size distribution of thermally etched ceramics was determined via the ImageJ software from about 500 grains per sample. Thermal etching was performed 10°C above the sintering temperature for 30 min in a nitrogen flow containing 10 % H₂S (to avoid oxidation from residual oxygen in the etching atmosphere). Due to the low reactivity of the pressureless sintering of CLS in the investigated temperature range³⁶, increase in grain size due to a thermal etching performed in a short time at only 10 °C above the sintering temperature is considered as negligible. The grain size distribution is defined by d10, d50 and d90 which are particle diameters where 10 %, 50 % and 90 % of the population is lying below these sizes, respectively.

The density of the sintered samples is the mean value of five measurements per test sample using Archimedes method in absolute ethanol (to accelerate drying between measurements) with a precision of about 1 %. The relative density (or densification rate) of the ceramics was calculated using a theoretical density of 4.574 g.cm⁻³ (determined from refined lattice constant $a = 8.6872 \text{ \AA}$). The relative density is based on the chemical composition of the unreduced CLS and fixed as same for all samples for simplification but it actually varies with the reduction of the compounds, without significant variation of the lattice parameter^{3, 30-35}. Micro-hardness of the sintered samples was determined using a micro-hardness tester MXT-70 (Matsuzawa® Seiki Co., Ltd., Japan) with a Vickers diamond indenter. Test load of 100 gf was applied perpendicularly to the polished surfaces. Holding time was 25 s. Values reported in Table 2 were averaged over five randomly performed indents.

3. RESULTS AND DISCUSSIONS

3.1. CLS powders

XRD patterns and FTIR spectra show that the synthesis procedure leads to the formation of well-crystallized and pure CaLa_2S_4 phase, free from impurity absorption bands (see Figures S1 and S2 in Supplemental Materials). As shown on SEM micrographs (Figure 1A), as-combusted powders consist of porous agglomerates made up of primary particles of different shapes and sizes, reflecting their compositional heterogeneity. One can observe 1-3 μm long and 100-200 nm thick needles, large 100-500 nm thick plate-like particles and rounded nanometric sized (<500 nm) particles. After sulfurization, the powder morphology is significantly modified (Figure 1B). The primary particles of uniform rounded shape and nanometric size are partially sintered and form large porous structures of several microns. The SSA decreased from $6 \text{ m}^2.\text{g}^{-1}$ to $1 \text{ m}^2.\text{g}^{-1}$ upon thermal treatment. Particle-size distribution measurements of the CLS powders show a multi-modal broad particle size distribution, ranging from 0.05 to 30 μm . The majority modes are centered on 15 μm and 3-5 μm , corresponding, respectively, to large and small agglomerates, as observed in Figure 1B, made up of primary particles of size centered on 0.2-0.5 μm (laser diffraction data are reported in Figure S3 in the Supplemental Materials).

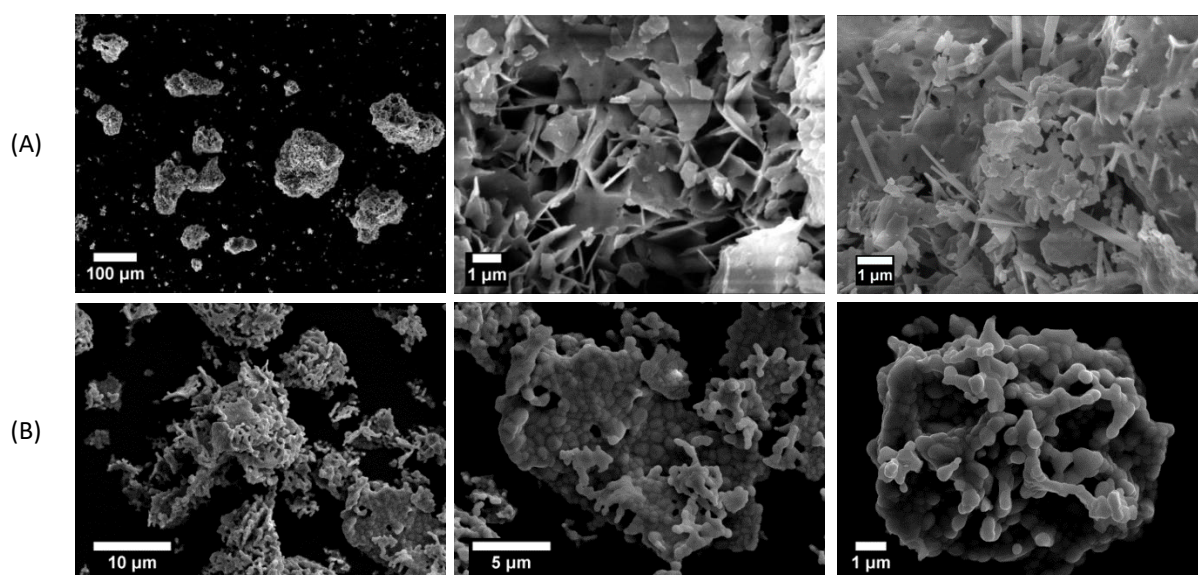


Figure 1: Secondary electron SEM micrographs of powders (A) before (as-combusted) and (B) after sulfurization (CLS)

3.2. CLS ceramics sintered by FAST

(A) Characterization

Table 1 reports the experimental sintering parameters, relative density and photographs of FAST sintered samples. Sintering was carried out at the optimized temperature of 1000°C to prevent the material reduction. This issue is further addressed in Section 3.3.(B). Photographs reveal, for all samples, the presence of cracks, parallel to the loading axis. After removal of the Papyex® foil by polishing, pellets fell into small pieces. Density of sintered samples was measured on the biggest pieces using Archimedes method. Due to the small size (low weight) of the fragments, the density of FAST sintered samples is measured with relatively low precision (error bars plotted in Figure 2). XRD patterns of the ceramic samples are similar to that reported for HP samples (see Figure S4 in Supplemental Materials). As regards to the macro and micro-fragmentation (see Figure S5 in Supplemental Materials), Vickers hardness measurements (by micro-indentation) were not relevant for FAST samples and could not be compared to those of HP samples.

Table 1: Sintering parameters, relative density and visual aspect of FAST sintered CLS samples

* Photographs under low-angled (non perpendicular) light





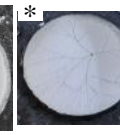
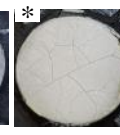


Sample	FAST1	FAST2	FAST3	FAST4	FAST5	FAST6	FAST7	FAST8
Temperature (°C)	1000	1000	1000	1000	1000	1000	1000	1000
Pressure (MPa)	12	40	60	80	80	80	80	80
Dwell time (min)	27	15	15	15	15	10	9	3.5
Heating rate (°C.min ⁻¹)	50	50	50	50	10	150	250	350
Total process duration (min)	47	35	35	35	115	17	13	6.5
Density (% theor.)	83 %	98 %	96 %	> 99 %	98 %	98 %	97 %	98 %
Visual aspect Diam. = 18mm + graphite foil								

Figure 2 shows the relative density of FAST sintered samples as a function of applied load with a constant heating rate of 50°C.min⁻¹. Figure 3 displays SEM micrographs of thermally etched surfaces of the corresponding ceramics. A significant increase in relative density is observed between 12 MPa (minimum load) and 40 MPa where it reaches 98 % (± 1 %). The increase in relative density is thereafter negligible between 40 MPa and 80 MPa considering the measurement precision.

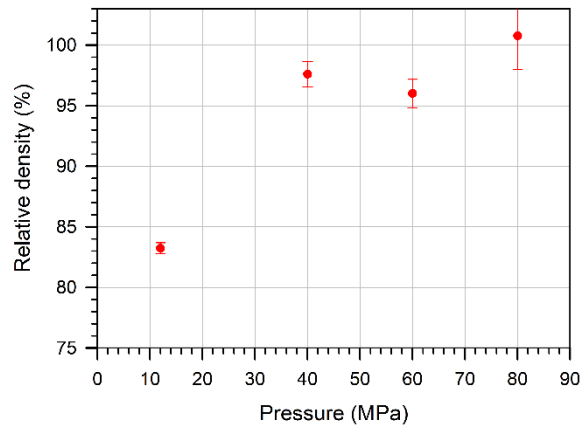


Figure 2: Relative density of FAST sintered ceramics as a function of applied load (heating rate: $50^{\circ}\text{C}\cdot\text{min}^{-1}$)

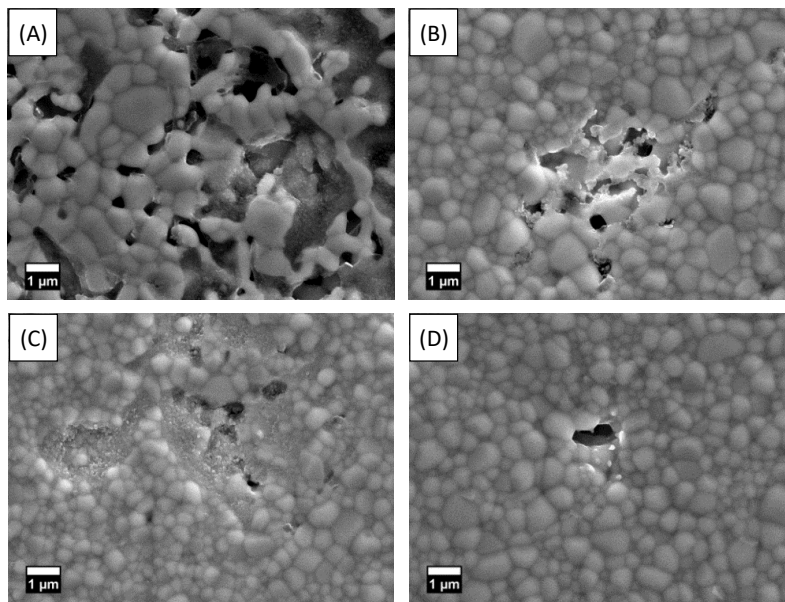


Figure 3: Secondary electron SEM micrographs of etched surfaces of FAST ceramics sintered under (A) 12 MPa-FAST1 (B) 40 MPa-FAST2 (C) 60 MPa-FAST3 (D) 80 MPa-FAST4 (heating rate: $50^{\circ}\text{C}\cdot\text{min}^{-1}$)

Figure 3A shows that sintering under 12 MPa has merely proceeded to the intermediate stage (large and open porosity) which is consistent with a relative density of 83 %. Application of loads ≥ 40 MPa intensifies the densification process to the final stage of sintering (isolated porosity) with a relative density of 98 % (Figure 3B-D). The maximum relative density is attained under 80 MPa and 15 min dwell time. The microstructure of the ceramics is typical of a single-phase polycrystalline material. The grains are all of polyhedral shape with size ranging from 0.3 to 1 μm .

Grain size distributions (determined via the ImageJ software) are plotted on Figure 4 as a function of applied load and heating rate. One can see that grain size of samples densified to ≥ 97 % does not vary much with applied pressure. In general, coarsening or grain growth occurs during sintering but it can be

minimized due to the applied pressure⁴¹ as it is observed under applied load of ≥ 40 MPa. Similarly, heating rate has no effect on the grain size. In fact, increasing the heating rate makes the sintering proceed more rapidly (as evidenced by smaller dwell times) resulting in a finer microstructure at the sintering temperature. However even for FAST5 and FAST8 samples, respectively sintered at 10 and $350^{\circ}\text{C}\cdot\text{min}^{-1}$ or for 115 min and 6.5 min, the grain size is similar. It is suggested that the total duration of the process is too short to observe a significant grain growth. As a result, the grain size remains sub-micrometric and is not much affected by the sintering conditions (80 MPa, 1000°C) which satisfy the compromise between required pore closure and undesirable grain growth.

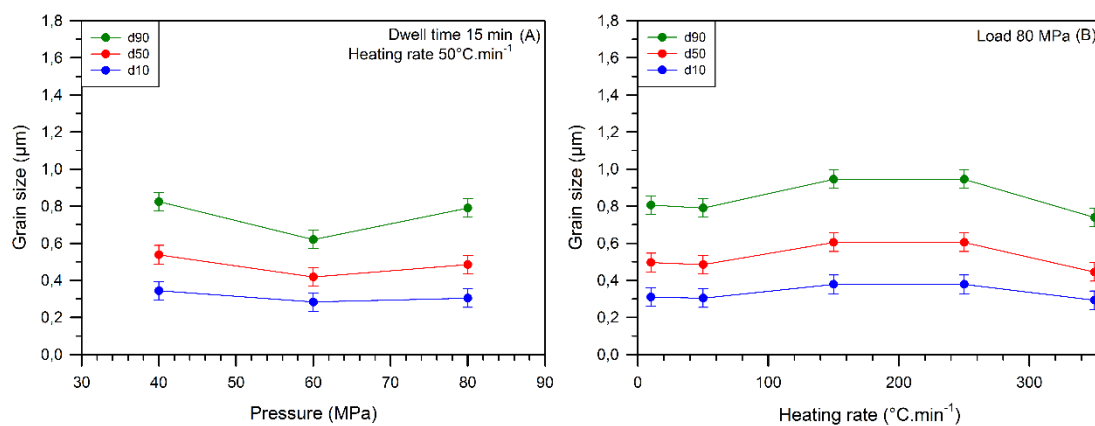


Figure 4. Grain size of FAST ceramics as a function of (A) applied load (heating rate: $50^{\circ}\text{C}\cdot\text{min}^{-1}$) and (B) heating rate (load: 80 MPa)

(B) Optical transmission

Figure 5 shows the infrared transmission spectra of the FAST ceramics with the same thickness of 1.4 mm, as a function of applied load at a heating rate of $50^{\circ}\text{C}\cdot\text{min}^{-1}$. It can be observed that the transmission is very low for dense ceramics sintered under ≥ 40 MPa (FAST2, FAST3, FAST4) and zero for the ceramic sintered under 12 MPa (FAST1) as expected from its low density (83 %). The increase in transmission with applied pressure indicates a better densification that is consistent with the elimination of residual porosity observed by SEM and density values. The best transmission level is obtained at 80 MPa with a maximum transmission of 3 % at around $14 \mu\text{m}$. It is noteworthy that the absorption band at about $11 \mu\text{m}$, characteristic of SO_3^{2-} group^{3, 26}, identifies the presence of residual oxygen.

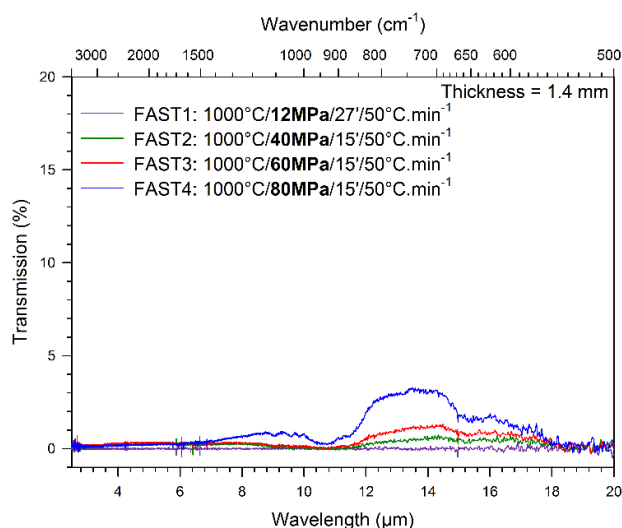




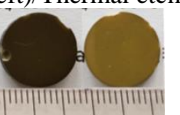
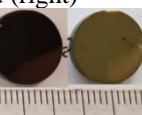
Figure 5: Infrared transmission of FAST ceramics as a function of applied load

3.3. CLS ceramics sintered by HP

(A) Characterization

HP was conducted by varying the sintering temperature between 800°C and 1100°C with fixed applied pressure (120 MPa), dwell time (6 h) and heating rate (10°C.min⁻¹). Table 2 reports the experimental sintering parameters, relative density, Vickers hardness and photographs of HP sintered samples. The photographs show a gradual darkening with the increase of the sintering temperature: at 800°C, the ceramics are of the same pale yellow color as the initial powder while at 1100°C the ceramics are completely black. The increase in density is significant between 800°C and 900°C and becomes negligible above 900°C with regard to the measurement precision.

Table 2: Sintering parameters, relative density and visual aspect of HP sintered CLS samples

Sample	HP1	HP2	HP3	HP4
Temperature (°C)	800	900	1000	1100
Pressure (MPa)	120	120	120	120
Dwell time (h)	6	6	6	6
Heating rate (°C.min ⁻¹)	10	10	10	10
Density (% theor.)	88.1	99.5	99.6	99.7
Vickers Hardness (kg.mm ⁻²)	83 ± 8	570 ± 14	621 ± 26	582 ± 11
Visual aspect (Scale cm/mm)				

XRD patterns of the ceramics hot pressed at 800°C and 900°C are comparable to that of the initial pure CLS powder (Figure 6). β -La₂S₃ was detected as a minor phase in XRD patterns of ceramics sintered at 1000°C and 1100°C. This phase is a pseudo-allotrope (low temperature phase) of γ -La₂S₃,

stabilized by residual oxygen (actually an oxysulfide of chemical formulation $\text{La}_{10}\text{S}_{14}\text{O}^{27}$). $\beta\text{-La}_2\text{S}_3$ forms in presence of oxygen concentration as low as 500 ppm⁴²⁻⁴⁴ and is consequently currently observed as impurity in CLS materials^{22, 24}. Its contribution to the material optical properties is further addressed in Section 3.3(B).

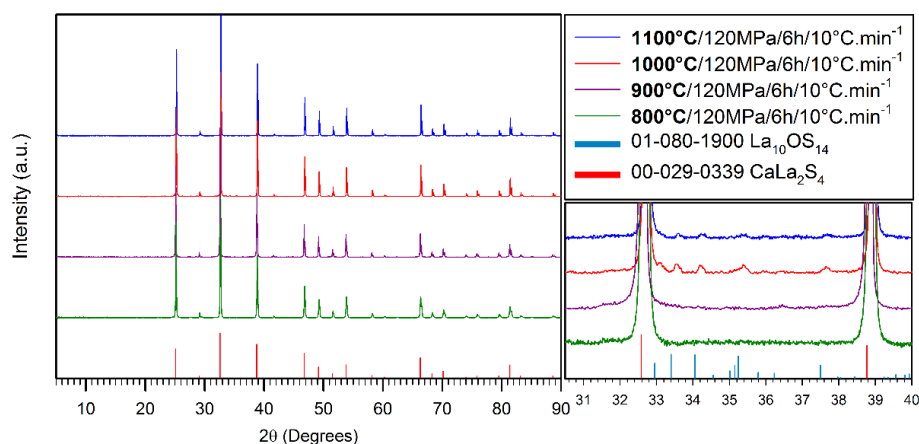


Figure 6: XRD patterns of the HP CLS ceramics sintered at various temperatures

Backscattered electron micrographs (BSE-SEM) of polished samples (before thermal etching) show some bright particles for ceramics HPed at $T \geq 900^\circ\text{C}$ (Figure 7). These are characteristics of electron denser areas. Particle size analysis via ImageJ of the center of the image (C), labeled in red, indicates that the medium size (diameter) of these bright particles is $0.9 \mu\text{m}$. The black spots in the images are due to porosity.

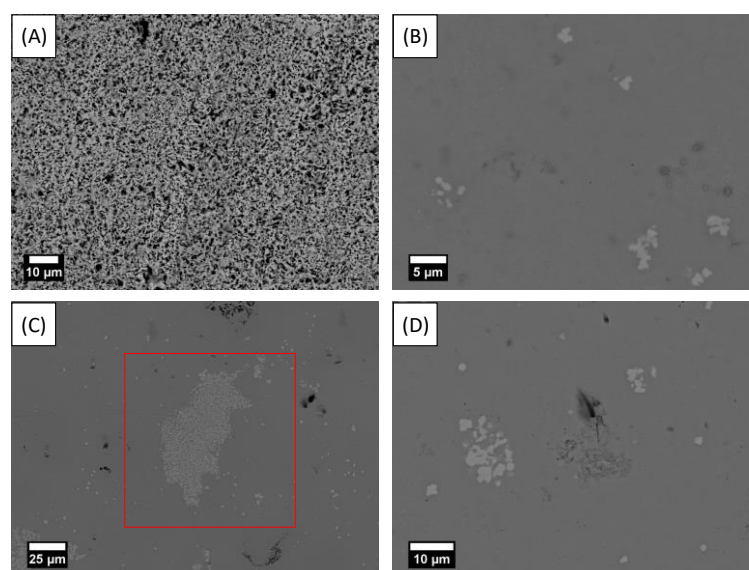


Figure 7: BSE-SEM micrographs of polished surfaces of ceramics HPed at (A) 800°C (HP1), (B) 900°C (HP2), (C) 1000°C (HP3) and (D) 1100°C (HP4)

EDS analysis (Table 3) reveals the presence of a lanthanum-rich secondary phase (bright particles) dispersed in a calcium-rich matrix, as reported in previous work²⁵. The composition of the matrix matches well the theoretical composition of CLS with La/Ca=2.3 ($\text{Ca}_{0.90}\text{La}_{2.07}\text{S}_4$). Due to the size of the bright particles (from 0.2 μm to few micrometers), EDS composition of this area could be that of a mixture of a lanthanum-rich area and a calcium-rich matrix (the volume analyzed is roughly a sphere of 1 μm^3). As regards to the accuracy of the measurement, this second phase could be $\beta\text{-La}_2\text{S}_3$, also detected by XRD (HP3 and HP4), or some reduced phase $\text{La}_3\text{S}_4\cdot\text{Ca}$ which could not be detected by XRD. As mentioned earlier, La_3S_4 and CLS are isostructural with similar lattice constants^{33–35}.

Table 3: EDS analysis of ceramics HPed at 800°C (HP1), 900°C (HP2), 1000°C (HP3) and 1100°C (HP4)

Sample	Composition (Atm %)	SEM-EDS	
		Dark phase	Bright phase
HP1	Ca	12.8 ± 1 %	undetected
	La	29.7 ± 1 %	undetected
	S	57.5 ± 1 %	undetected
HP2	Ca	12.8 ± 1 %	4.6 ± 1 %
	La	29.6 ± 1 %	37.0 ± 1 %
	S	57.7 ± 1 %	58.4 ± 1 %
HP3	Ca	12.0 ± 1 %	4.5 ± 1 %
	La	29.9 ± 1 %	36.7 ± 1 %
	S	58,1 ± 1 %	58.8 ± 1 %
HP4	Ca	12.8 ± 1 %	1.6 ± 1 %
	La	29.7 ± 1 %	40.0 ± 1 %
	S	57.5 ± 1 %	58.4 ± 1 %

Figure 8 shows the SEM micrographs of thermally etched surfaces of the HP ceramics sintered at 800°C, 900°C, 1000°C and 1100°C. The micrographs reveal dense microstructures at sintering temperatures $\geq 900^\circ\text{C}$ with some residual porosity at grain boundaries (spotted by red arrows). Mean grain size increases with sintering temperature from about 0.5 μm at 800°C to 0.9 μm at 1100°C. The best compromise in terms of relative density and grain size is thus observed at 1000°C.

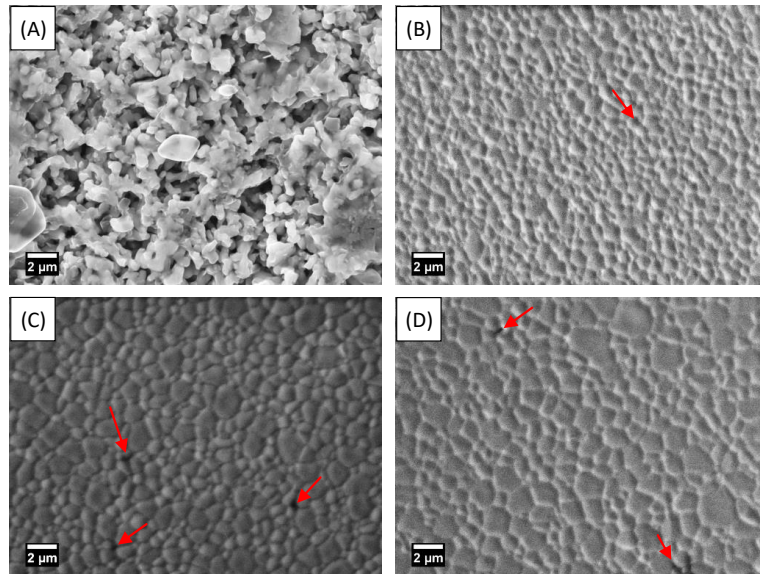


Figure 8: Secondary electron SEM micrographs of etched surfaces of HP ceramics sintered at (A) 800°C (HP1) (B) 900°C (HP2) (C) 1000°C (HP3) and (D) 1100°C (HP4)

Grain size distributions (determined from SEM micrographs via the ImageJ software) are plotted on Figure 9 as a function of the sintering temperature. It is observed that d10 and d50 increase linearly with temperature. On the other hand, a change in slope is observed in the evolution of d90 at sintering temperatures above 900°C, indicating a net increase in the population of “large” grains. Nevertheless, grain growth remains somewhat limited between 900°C and 1100°C where 98 % of the population is smaller than 2 μm. This results in a negligible change in hardness values as regards to the standard deviation (Table 2). These values are consistent with the ones reported in the literature^{3, 29}.

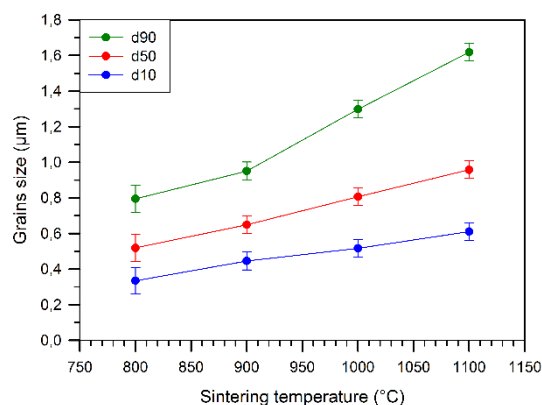


Figure 9: Grain size of HP ceramics as a function of sintering temperature

(B) Optical transmission

Figure 10 shows the IR transmission spectra of the HP ceramics (th = 1.9 mm) sintered at 800°C, 900°C, 1000°C and 1100°C.

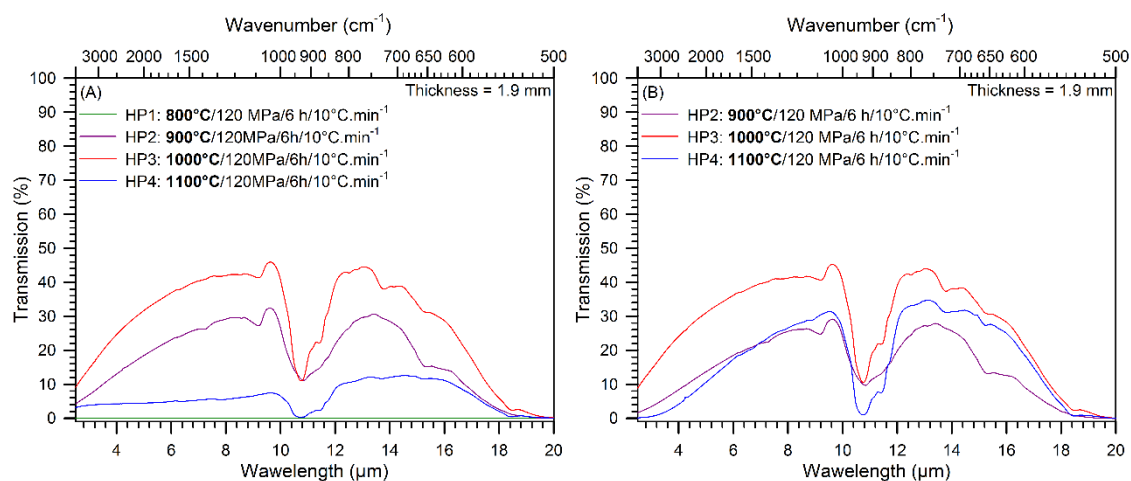


Figure 10: Infrared transmission of (A) as-HPed and (B) thermal etched HPed ceramics






One can observe that the influence of sintering temperature on the level of transmission is significant. As expected from its low relative density (88 % of theoretical density), the sample sintered at 800°C does not exhibit any transmission in the investigated wavelength range. The increase in temperature from 800°C to 1000°C allows for a marked increase in transmission, reaching 44 % at 13 μm . This result is consistent with a decrease in porous volume attested by the 99.6 % relative density. The low transmission level of sample sintered at 1100°C is assumed to be due to a reduction phenomenon induced by the graphitic sintering atmosphere. This hypothesis is confirmed by the thermal etching of the samples for 30 min in nitrogen containing 10 % H_2S at 10°C above the HP set temperature. This treatment had no significant impact on the optical properties of samples sintered at 900°C and 1000°C but drastically increased the transmission level of the sample sintered at 1100°C. This finding supports the idea that this sample has experienced some severe reduction during HP giving a shift of the composition towards a sulfur-deficient $\text{La}_3\text{S}_4\text{:Ca}$ phase, isostructural to CLS. Sulfur deficiency causes transmission loss due to free carriers absorption^{25, 37}. To explain the reduction phenomenon, Chess et al.⁶ propose a mechanism by contact with the graphite of the mold. Alternatively, we showed that the reduction could be induced by the graphitic environment independently of any contact³⁶. The reduction is then assumed to arise from a CO-containing residual atmosphere that forms in contact with any traces of oxygen present in the hot-press and/or in the graphite felts. Sulfur stoichiometry is partially restored upon thermal etching and IR transmission is thereby improved (sample HP4, Figure 10B). In addition, transmission spectra present, as observed for FAST samples, absorption bands centred at 11 μm and 9 μm attributed to sulfate species^{3, 26} which form in presence of residual oxygen or originate from β -

La_2S_3 phase detected as a minor phase in XRD patterns of ceramics sintered at 1000°C and 1100°C . Let us note that this secondary phase does not significantly affect the infrared transmission level.

3.4. Comparison FAST/HP techniques

HP and FAST techniques were further assessed in the production of transparent CLS ceramics using the same conditions of pressure (80 MPa) and dwell time (15 min). Two heating rates (10 and 50°C.min⁻¹) were applied for both techniques and one FAST cooling rate was controlled at 10°C.min⁻¹. Table 4 reports the experimental sintering parameters, relative density and photographs of sintered samples.

Table 4: Sintering conditions, relative density and visual aspect of CLS ceramics sintered by FAST and HP

Sample	FAST5	FAST4	FAST9	HP5	HP6
Temperature (°C)	1000	1000	1000	1000	1000
Pressure (MPa)	80	80	80	80	80
Dwell time (min)	15	15	15	15	15
Heating rate (°C.min ⁻¹)	10	50	50	10	50
Cooling rate (°C.min ⁻¹)	*	*	10	*	*
* natural cooling					
Density (% theor.)	98	> 99	> 99	98.1	99.0
Visual aspect (Scale cm/mm)					

First, while HP allows the production of non-fractured ceramics in most cases, FAST precludes it, despite the large variety of conditions examined including the application of a relatively slow cooling rate of 10°C.min⁻¹. In addition, in that particular case (FAST 9), it is observed that the ceramic undergoes the same blackening as the one observed with HP ceramics sintered for 6 h implying that the same reduction phenomenon operates in FAST. Color and homogeneity of ceramics are similar with both techniques. Relative density and grain size are also comparable. For example, grain size of HP5 ranging from 0.4 to 0.8µm (0.35/0.52/0.81µm - d10/d50/d90) is very similar to that of FAST5 (0.31/ 0.50/ 0.81 µm) sintered in the same conditions by FAST.

Figure 11 compares IR transmission of FAST and HP ceramics (th = 1.4 mm), sintered in the conditions reported in Table 4. Despite sintering conditions far from the optimized ones for HP as previously determined (1000°C, 120 MPa, 6 h), HP ceramics still have higher transmission than FAST ceramics. We observe a slightly higher transmission for FAST5 sample, in comparison to FAST4 sample

sintered at the same temperature and pressure conditions, which we attribute to a better relative density that unfortunately cannot be accurately measured on fragments.

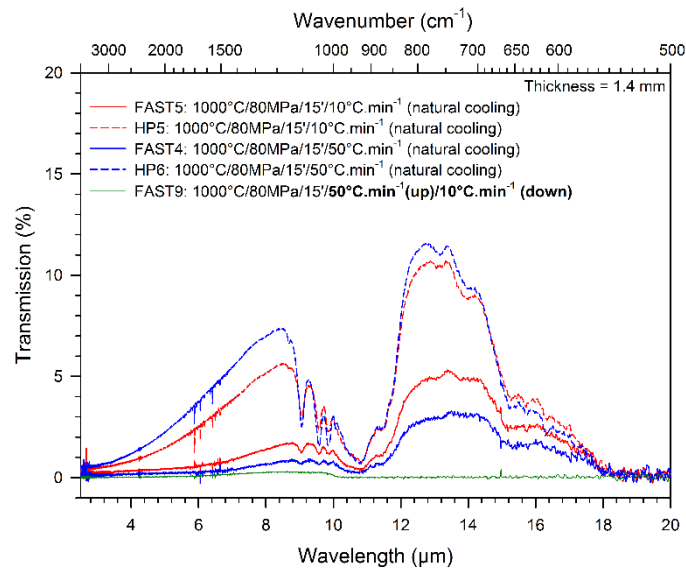


Figure 11: Infrared transmission of FAST and HP CLS ceramics sintered in the same conditions

Our experimental results are consistent with the literature data^{4, 6, 10, 13}. The best optical performance is obtained when HP is applied at 1000°C for 6 h under 120 MPa. The transmission reaches 40 % to 45 % ($t_h = 1.9\text{mm}$) in the 8-14 μm window, for 69 % in theory, despite the presence of a $\text{La}_3\text{S}_4:\text{Ca}$ opaque phase lowering the transmission level in the entire wavelength range.

We retain though that FAST technique results in fragmentation of the CLS ceramics. Note this issue was not mentioned in the work of Li et al.²⁹ who reported comparable sintering conditions for commercial CLS powders. The difference between HP and FAST techniques lies in the way the heat is produced and transmitted to the material. This suggests the issue may be related to effects induced by the DC pulse sequences. Our assumption is that with sulfur loss shifting the composition towards $\text{La}_3\text{S}_4:\text{Ca}$, the nature of conductivity changes locally from dielectric to metallic. The dispersion of an electrically conductive phase within an electrically insulating one may induce current flows directly through the green body rather than through the graphite die. Possible interactions between current paths/hot spots and the insulating matrix can exceed the fracture strength of the samples⁴⁵. The hypothesis of the creation of conduction paths is favored over the hypothesis of the unique Joule heating characteristic of FAST (thermal gradients). Indeed, fragmentation occurs even under most favorable conditions (low heating and cooling rates) to limit thermal effects (especially on small samples).

Nevertheless, the second hypothesis can not be dismissed in absence of direct proof for the reason of the fragmentation. Future studies would involve a FAST configuration in which the current is forced to flow within the die only, to state on the influence of heat gradients and/or the supposedly conductive paths or hot spots due to the $\text{La}_3\text{S}_4\text{:Ca}$ phase.

4. CONCLUSIONS

FAST and HP techniques were employed to densify CLS powders prepared by combustion method. For FAST (at short dwell times and 1000°C), neither the pressure nor the heating rate have a significant impact on the grain size of the ceramics. For conventional HP, due to long dwell time (6h), the increase in sintering temperature, in the range 800°C - 1100°C , leads to a slight increase in grain size of the ceramics. Comparison of the two techniques (use of identical sintering parameters: 1000°C , 80 MPa, 15 min dwell time, heating rates of $10^\circ\text{C}\cdot\text{min}^{-1}$ and $50^\circ\text{C}\cdot\text{min}^{-1}$) shows that FAST and HP produce ceramics with comparable relative density and grain size, in the range of that of the primary particles of the powders) ($< 1\mu\text{m}$). Nevertheless, HP ceramics have higher transmission than FAST ceramics.

Moreover, we showed that CLS powders could not be densified by FAST without fragmentation, in the investigated conditions. The origin of the fragmentation could be related to the heating mode (DC pulses) and/or to thermal gradients due to the Joule heating of the graphite mold. Indeed, if the sintering conditions in graphitic atmosphere actually form sulfur-deficient phases ($\text{La}_3\text{S}_4\text{:Ca}$), the electrical behavior of CLS would be transformed into that of a kind of composite behavior making FAST electric effects detrimental to the mechanical integrity of the parts. But thermal gradients can not be excluded either in the absence of direct proof. Future work may explore these assumptions via the investigation of FAST on electrically isolated CLS.

A maximum optical transmission of 40-45% ($t_h = 1.9\text{ mm}$) was measured out of a possible maximum of 69% in the 8-14 μm window when HP is applied at 1000°C for 6 h under 120 MPa. Powder treatment in sulfurizing atmosphere prior to densification is though necessary to remove any trace of oxygen responsible for absorption bands. Still, the major encountered issue is the precipitation, as low as 1000°C , of $\text{La}_3\text{S}_4\text{:Ca}$ phases which compromise the achievement of the theoretical transmission. Resulfurization of the dense ceramics could partially compensate the reduction but has any impact on the elimination of residual oxygen trapped in the bulk. Future research will involve a pre-sintering in

sulfurized atmosphere to ensure the elimination of the residual oxygen prior to the porosity closure and a post-sintering by use of HIP graphite-free technique.

Acknowledgement

The authors are grateful to the French Direction Générale de l'Armement (DGA) and the industrial partner, Solcera Advanced Materials, Evreux, France, for their financial support (PhD grant, Dr G.R. Durand).

REFERENCES

1. Harris DC. Materials for Infrared Windows and Domes. SPIE Optical Engineering Press; 1999
2. Saunders KJ, Wong TY, Hartnett TM, Tustison RW, Gentilman RL. Current and Future Development of Calcium Lanthanum Sulfide. In: Schwartz RW, ed. *Proc. SPIE Vol. 0683 Infrared Opt. Transm. Mater.* Vol. 0683. San Diego, US: International Society for Optics and Photonics; 1986:72–78. <https://doi.org/10.1117/12.936418>
3. Chess DL, Chess CA, Marks JA, White WB. Phase equilibria and processing of infrared optical ceramics on the join $\text{CaLa}_2\text{S}_4\text{-La}_2\text{S}_3$. *J Ceram Process Res.* 2010;11(4):465–470.
4. White WB, Chess D, Chess CA, Biggers JV. CaLa_2S_4 : Ceramic Window Material For The 8 to 14 μm Region. *Proc. SPIE Vol. 0297 Emerg. Opt. Mater.* Vol. 0297. San Diego, US: International Society for Optics and Photonics; 1982:38–43. <https://doi.org/10.1117/12.932482>
5. Harris DC. Development of hot-pressed and chemical-vapor-deposited zinc sulfide and zinc selenide in the United States for optical windows. In: Tustison RW, ed. *Proc. SPIE Vol. 6545 Window Dome Technol. Mater. X.* Vol. 6545. Orlando, US: International Society for Optics and Photonics; 2007:654502. <https://doi.org/10.1117/12.716808>
6. Chess DL, Chess CA, Biggers JV, White WB. Processing Ternary Sulfide Ceramics: Powder Preparation, Sintering, and Hot-Pressing. *J Am Ceram Soc.* 1983;66(1):18–22. <https://doi.org/10.1111/j.1151-2916.1983.tb09960.x>
7. Saunders KJ, Gentilman RL. Optical Material and Process For Making the Same. U.S. Patent US 4,765,931. 1988.
8. Marian E. Hills. Preparation, Properties, and Development of Calcium Lanthanum Sulfide as 8- to 12-micrometer Transmitting Ceramic. Naval Weapons Center; 1989
9. Tsai MS, Hon MH. Phase formation and thermal stability of calcium lanthanum sulfide powder. *Ceram Int.* 1994;20(5):303–308. [https://doi.org/10.1016/0272-8842\(94\)90046-9](https://doi.org/10.1016/0272-8842(94)90046-9)
10. Tsai M-S, Hon M-H. Fabrication of calcium lanthanum sulfide ceramic by carbonate coprecipitating method. *Scr Metall Mater.* 1995;32(5):713–718. [https://doi.org/10.1016/0956-716X\(95\)91591-C](https://doi.org/10.1016/0956-716X(95)91591-C)
11. White WB. Ternary Sulfide Infrared Window Materials. First Annual Report to the Office of Naval Research; 1981
12. Beswick JA, Pedder DJ, Lewis JC, Ainger FW. New Infra-Red Window Materials. *Proc. SPIE Vol. 0400 New Opt. Mater.* Vol. 0400. Geneva, Switzerland: International Society for Optics and Photonics; 1983:12–20. <https://doi.org/10.1117/12.935470>
13. Chess DL, Chess CA, White WB. Precursor Powders for Sulfide Ceramics Prepared by Evaporative Decomposition of Solutions. *J Am Ceram Soc.* 1983;66(11):c205–c206. <https://doi.org/10.1111/j.1151-2916.1983.tb10574.x>
14. Lewis KL, Savage JA, Marsh KJ, Jones APC. Recent Developments In The Fabrication Of Rare-Earth Chalcogenide Materials For Infra-Red Optical Applications. *Proc. SPIE Vol. 0400 New Opt. Mater.* Vol. 0400. Geneva, Switzerland: International Society for Optics and Photonics; 1983:21–28. <https://doi.org/10.1117/12.935471>
15. Covino J, Harris DC, Hills ME, Loda RT, Schwartz RW. Development Of Calcium Lanthanum Sulfide As An 8-12 μm Transmitting Ceramic. *Proc. SPIE Vol. 0505 Adv. Opt. Mater.* Vol. 0505. San Diego, US: International Society for Optics and Photonics; 1984:42–46. <https://doi.org/10.1117/12.964624>
16. Messing GL, Zhang S-C, Jayanthi GV. Ceramic Powder Synthesis by Spray Pyrolysis. *J Am Ceram Soc.* 1993;76(11):2707–2726. <https://doi.org/10.1111/j.1151-2916.1993.tb04007.x>

17. Vaughan-Forster CM, White WB. Powder Preparation and Sintering Characteristics of Rare-Earth Sesquisulfide Ceramics. *J Am Ceram Soc.* 1997;80(1):273–276. <https://doi.org/10.1111/j.1151-2916.1997.tb02826.x>
18. Li Y, Zhang L, Wu Y. Synthesis and characterization of calcium lanthanum sulfide via a wet chemistry route followed by thermal decomposition. *RSC Adv.* 2016;6(41):34935–34939. <https://doi.org/10.1039/C6RA05912K>
19. Kumta PN, Risbud SH. Low temperature synthesis of cubic lanthanum sulfide (La₂S₃) powders. *Mater Sci Eng B.* 1989;2(4):281–286. [https://doi.org/10.1016/0921-5107\(89\)90005-6](https://doi.org/10.1016/0921-5107(89)90005-6)
20. Wang LH, Hon MH, Huang WL, Lin WY. Formation and densification of CaLa₂S₄ powders by sulfidization of metal alkoxides. *Mater Sci Eng B.* 1990;7(3):237–242. [https://doi.org/10.1016/0921-5107\(90\)90034-9](https://doi.org/10.1016/0921-5107(90)90034-9)
21. Han Y, Akinc M. Preparation of Calcium Lanthanum Sulfide Powders via Alkoxide Sulfurization. *J Am Ceram Soc.* 1991;74(11):2815–2819. <https://doi.org/10.1111/j.1151-2916.1991.tb06848.x>
22. Tsay BJ, Hsing Wang L, Hsiung Hon M. Formation and densification of CaLa₂S₄ powders by sulfidization of modified metal alkoxides in different atmospheres. *Mater Sci Eng B.* 2000;72(1):31–35. [https://doi.org/10.1016/S0921-5107\(99\)00515-2](https://doi.org/10.1016/S0921-5107(99)00515-2)
23. Wang LH, Hon MH, Huang WL, Lin WY. Sulphurization of coprecipitated carbonates for formation of CaLa₂S₄. *J Mater Sci.* 1991;26(18):5013–5018. <https://doi.org/10.1007/BF00549885>
24. Li P, Jie W, Li H. Influences of Hot-Pressing Conditions on the Optical Properties of Lanthanum Sulfide Ceramics. *J Am Ceram Soc.* 2011;94(4):1162–1166. <https://doi.org/10.1111/j.1551-2916.2010.04243.x>
25. Merdignac-Conanec O, Durand G, Walfort S, Hakmeh N, Zhang X. Elaboration of CaLa₂S₄ transparent ceramics from novel precursor powders route. *Ceram Int.* 2017;43(8):5984–5989. <https://doi.org/10.1016/j.ceramint.2017.01.132>
26. Tsay BJ, Wang LH. A study on infrared transmission of lanthanum sulfide and oxysulfide in the 2.5–14 μm region. *Mater Lett.* 1998;34:180–183.
27. Wang LH, Hon MH, Huang WL, Lin WY. Phase development in the formation of CaLa₂S₄ powder and pellet. *Ceram Int.* 1992;18(1):27–33. [https://doi.org/10.1016/0272-8842\(92\)90058-L](https://doi.org/10.1016/0272-8842(92)90058-L)
28. Li Y, Zhang L, Kisslinger K, Wu Y. Field-Assisted Sintering and Phase Transition of ZnS-CaLa₂S₄ Composite Ceramics. *J Eur Ceram Soc.* 2017;37(15):4741–4749. <https://doi.org/10.1016/j.jeurceramsoc.2017.07.009>
29. Li Y, Wu Y. Sintering behavior of calcium lanthanum sulfide ceramics in field-assisted consolidation. *J Am Ceram Soc.* 2017;100(11):5011–5019. <https://doi.org/10.1111/jace.15027>
30. Lugev SM, Lugeva NV, Ismailov SM. The Debye temperature and Grüneisen parameter of the CaLa₂S₄-La₂S₃ system. *Phys Solid State.* 2002;44(6):1067–1070. <https://doi.org/10.1134/1.1485009>
31. Lugev SM, Lugeva NV, Ismailov SM. Thermal Conductivity, Thermal Expansion, and Microhardness of CaLa₂S₄-La₂S₃ Solid Solutions. *Inorg Mater.* 2002;38(4):339–343. <https://doi.org/10.1023/A:1015193519534>
32. Flahaut J, Domange L, Patrie M. Combinaisons formée par les sulfures des éléments du groupe des terres rares : IV) Étude cristallographique des phases ayant le type structural du phosphate de thorium Th₃P₄. *Bull Société Chim Fr.* 1962;11–12(340):2048–2054.
33. Picon M, Domange L, Flahaut J, Guittard M, Patrie M. Les sulfures Me₂S₃ et Me₃S₄ des éléments de terres rares. *Comptes Rendus Académie Sci Paris.* 1960;V 1-3:221–228.
34. Ivanchenko LA, Marchenko VI, Paderno YB, Serdyuk VA, Evdokimova VV, Novokshanov VI. Optical properties of and chemical bonds in lanthanum sulfide of variable composition. *Sov Powder Metall Met Ceram.* 1981;20(1):53–56. <https://doi.org/10.1007/BF00791911>
35. Takeshita T, Jr KAG, Beaudry BJ. Preparation of γ-LaS_y (1,33 < y < 1,50) alloys by the pressure-assisted reaction sintering method and their thermoelectric properties. *J Appl Phys.* 1985;57(10):4633–4637. <https://doi.org/10.1063/1.335373>
36. Durand G. Élaboration de céramiques transparentes de CaLa₂S₄ pour applications optiques dans l'infrarouge. thesis; Thèse de l'Université de Rennes 1; Rennes; 2017. <http://www.theses.fr/2017REN1S155>
37. Kamarzin AA, Mironov KE, Sokolov VV, Malovitsky YuN, Vasil'yeva IG. Growth and properties of lanthanum and rare-earth metal sesquisulfide crystals. *J Cryst Growth.* 1981;52(Part 2):619–622. [https://doi.org/10.1016/0022-0248\(81\)90351-1](https://doi.org/10.1016/0022-0248(81)90351-1)
38. Hakmeh N, Merdignac-Conanec O, Zhang X. Method of manufacturing a sulfide-based ceramic element particularly for IR-optics applications. European Patent Application EP 2 966 051 A1. 2016.
39. Singh SS, Pratap S, Prasad J, Kumar R, Murari K. Infrared (8–12 μm) Dome Materials: Current Status. *Def Sci J.* 1998;48(2):173–183. <https://doi.org/10.14429/dsj.48.3897>
40. Bayya S, Gibson D, Nguyen V, Fleet E, Vizgaitis J, Sanghera J. Multispectral optics designs using expanded glass map. In: Andresen BF, Fulop GF, Hanson CM, Norton PR, eds. *Proc. SPIE Vol. 9070 Infrared Technol. Appl. XL.* Vol. 90702G. Baltimore, US: International Society for Optics and Photonics; 2014:90702G. <https://doi.org/10.1117/12.2050624>

41. Fang ZZ, Wang H. 17 - Sintering of ultrafine and nanosized particles. In: Fang ZZ, ed. *Sinter. Adv. Mater.* Woodhead Publishing; 2010:434–473. <https://doi.org/10.1533/9781845699949.3.434>
42. Daniel Carré, Pierre Lauruelle, Pierre Besançon. Structure cristalline de la prétendue variété bêta des sulfures de terres rares de composition $\text{Pr}_{10}\text{S}_{14}\text{O}$. *Comptes Rendus Académie Sci Paris.* 1970;270(Série C):537–600.
43. Banks E, Stripp KF, Newkirk HW, Ward R. Cerium(III) Sulfide and Selenide and Some of their Solid Solutions. *J Am Chem Soc.* 1952;74(10):2450–2453. <https://doi.org/10.1021/ja01130a002>
44. Besançon P. Teneur en oxygène et formule exacte d'une famille de composés habituellement appelés "variété β " ou "phase complexe" des sulfures de terres rares. *J Solid State Chem.* 1973;7(2):232–240. [https://doi.org/10.1016/0022-4596\(73\)90159-X](https://doi.org/10.1016/0022-4596(73)90159-X)
45. Guillon O, Gonzalez-Julian J, Dargatz B, *et al.* Field-Assisted Sintering Technology/Spark Plasma Sintering: Mechanisms, Materials, and Technology Developments. *Adv Eng Mater.* 2014;16(7):830–849. <https://doi.org/10.1002/adem.201300409>